Symmetry breaking in pseudomorphic V-groove quantum wires

M. Grundmann, O. Stier, and D. Bimberg
Institut für Festkörperphysik, Technische Universität Berlin, Hardenbergstraße 36, D-10623 Berlin, Germany
(Received 20 June 1994)

Pseudomorphic crescent-shaped quantum wires are shown to exhibit size-dependent symmetry breaking due to an anisotropic strain distribution. We predict level degeneracies and an increased carrier lifetime. As a model system $In_{0.2}Ga_{0.8}As/Al_{0.2}Ga_{0.8}As$ quantum wires are simulated with finite-element analysis to obtain the strain tensor. Within the confinement potentials, which are strongly modified by the strain-induced potentials and the piezoelectric field, the single-particle Schrödinger equation is solved for electrons and holes.

The physics and application of quantum wells (QW's) have been leading towards more flexible design[1] and improved device performance[2,3] by the use of lattice-mismatched materials. The same trend is now foreseeable in the field of one- and zero-dimensional nanostructures which originally started out from lattice-matched material combinations.[4,5] Strained nanostructures have been reported as being useful for quantum wire (QWR) lasers with a wavelength range not accessible with lattice-matched materials,[6,7] and the self-organized growth of quantum-dot arrays.[8–10] Also strain-induced lateral potential modulation has been used for fabrication of QWR's.[11,12]

QWR's grown *in situ* into V grooves exhibit very high optical quality[13,14] and are one of the most attractive QWR systems for practical laser application.[4] In this paper we present a detailed treatment of the effects of strain on V-groove QWR's. A size-dependent symmetry breaking of the hole wave-function impacting the electronic levels and the recombination properties is observed.

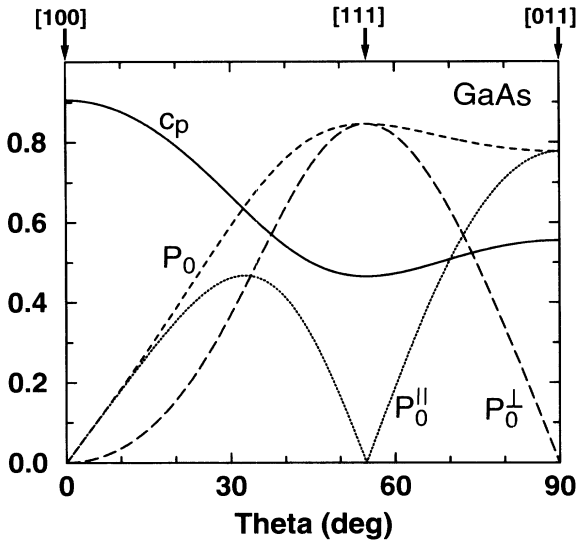

FIG. 1. Normalized contraction $c_p = -\varepsilon_\perp/\varepsilon_\parallel$ (solid line), normalized amplitude of the piezoelectric polarization $P_0 = |\mathbf{P}|/(e_{14}^*\varepsilon_\parallel)$ (short dashed line), and components parallel ($P_0^\parallel$, dotted line) and perpendicular ($P_0^\perp$, long dashed line) to the interface plane for GaAs material parameters. Variation of crystallographic direction for azimuth of 45°.

The effect of lattice-mismatched induced strain in pseudomorphic quantum *wells* is described by interfacial strain $\varepsilon_\parallel$ and perpendicular strain $\varepsilon_\perp = -\varepsilon_\parallel c_p$ due to the Poisson effect. The perpendicular contraction c_p depends on the crystallographic orientation of the interface plane and the elastic constants of the well material and is shown for GaAs material parameters in Figs. 1 and 2. The barriers of a quantum well remain completely unstrained.[15] The situation for a V-groove quantum *wire* is more complicated due to the additional nontrivial constraints in the growth direction. For our simulation we use a crescent-shaped wire geometry. In the following, z represents the [001] growth direction and x the lateral coordinate along [110] when the QWR extends along y parallel to $[1\bar{1}0]$.

We expect the strain to be mostly *hydrostatic* in character in the bottom center because there the constraints in all three directions are largest. On the contrary, at the top interface the QWR appears to be most similar to a

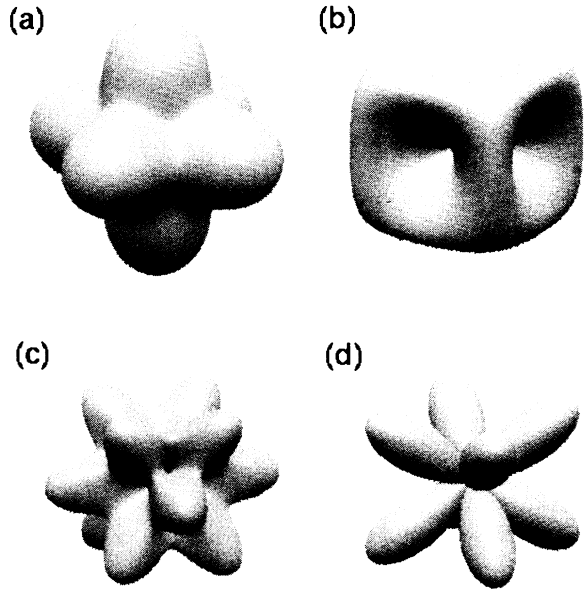

FIG. 2. Three-dimensional visualization of c_p (a), P_0 (b), $P_0^\parallel$ (c), and $P_0^\perp$ (d). For a description of symbols see caption of Fig. 1 and text. ⟨100⟩ directions are along maxima in (a), ⟨111⟩ directions are along maxima in (d).

0163-1829/94/50(19)/14187(6)/$06.00

quantum well, so there we expect the *anisotropic* part of the strain tensor to be large. A detailed analysis, however, can only be done numerically. We employ a finite-element analysis of cubic materials to obtain the strain tensor. We like to emphasize that the pattern of the strain distribution depends only on the *shape* of the QWR but not on its particular *size*.

As is well known,[16,17] strain induces a modification of the conduction and valence bands, namely, a shift E_0 of the fundamental band gap proportional to the isotropic part of the strain tensor,

$$E_0 = -a(\varepsilon_{xx}+\varepsilon_{yy}+\varepsilon_{zz}) = -a\,\mathrm{Tr}\underline{\varepsilon} \quad (1)$$

and valence-band splitting E_1 given by the anisotropic part of the strain tensor due to biaxial and shear strains (neglecting second-order corrections due to the split-off hole band[16,18])

$$E_1^2 = \frac{b^2}{2}[(\varepsilon_{xx}-\varepsilon_{yy})^2+\text{cycl.}]+d^2[\varepsilon_{xy}^2+\text{cycl.}] \quad (2)$$

with a, b, and d being the hydrostatic and shear deformation potentials, respectively.

The shear strains ε_{jk}, $j\neq k$ additionally introduce a piezoelectric polarization field $P_i = e_{14}\varepsilon_{jk}$, $i\neq j\neq k$, via the piezoelectric modulus e_{14}.[19] Due to symmetry the field lies within the $(1\bar{1}0)$ wire cross-section plane. The importance of the piezoelectric effect is well known from strained QW's (Ref. 20) and superlattices[21] on (111)-oriented substrates. The field direction depends on the polar orientation of the crystal (compression in the [111] direction leads to positive charging of the A faces (metal atoms)). The amplitude of the piezoelectric polarization depends on the crystal orientation as shown in Figs. 1 and 2 for GaAs and arbitrary directions.

The piezoelectric polarization **P** induces a fixed charge density $\rho_P = -\mathrm{div}\mathbf{P}$, which is mainly concentrated at the interfaces, the upper interface being charged positively for a compressed QWR along $[1\bar{1}0]$, negatively for a QWR along [110]. Charge carriers in the QWR are thus subjected to a spatially varying potential

$$V_P(r) = (1/4\pi\varepsilon_0\varepsilon_r)\int\int\int[\rho_P(r')/|r-r'|]d^3r'. \quad (3)$$

In the following we use as a model material $In_xGa_{1-x}As$ QWR's which have found considerable interest.[7,22–24] As barrier material we take $Al_{0.2}Ga_{0.8}As$. The lattice mismatch for $x=0.2$ is $\varepsilon=1.4\%$. The elastic coefficients C_{ij} and the deformation potentials used in the calculations are given in Table I. The strains obtained from the finite-element simulation are shown in Fig. 3.

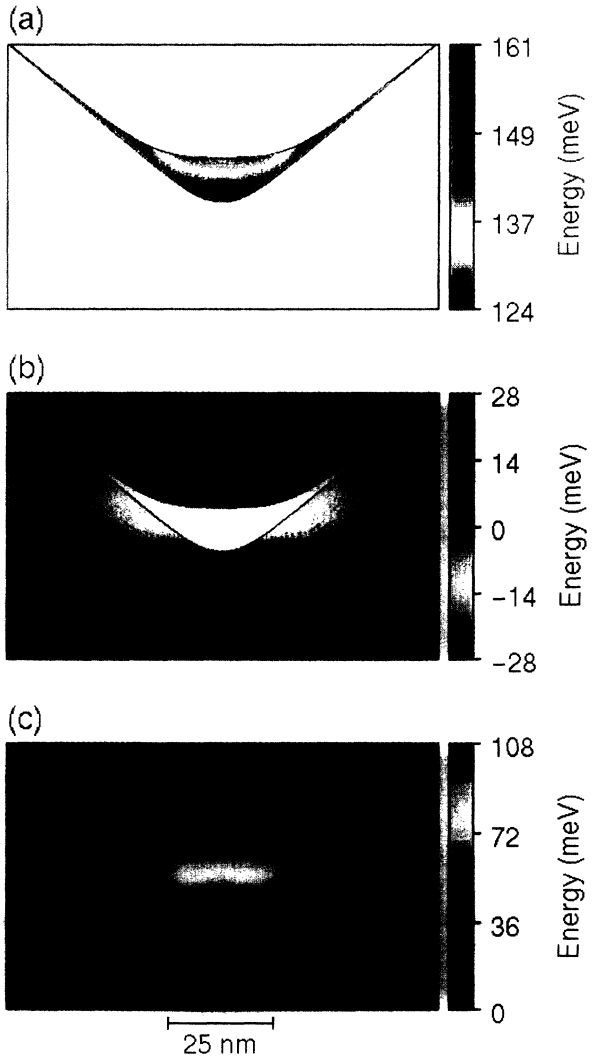

FIG. 3. Hydrostatic band shift in the wire (a), and in the barrier (b), and valence-band splitting (c) for an $In_{0.2}Ga_{0.8}As/Al_{0.2}Ga_{0.8}As$ quantum wire. Color scale for (c) is reversed because larger valence-band splitting means lower hole ground-state energy.

The hydrostatic band shift is largest, as expected, in the bottom center of the V groove and exhibits several tens of meV modulations across QWR. Also the band-gap splitting shows a distinct variation with the minimum value in the bottom center. To obtain the electron and hole confinement potentials ΔE_e and ΔE_h, the strain-induced changes have to be added to the heterostructure band offsets. The offset ratio Q_0 for the unstrained bands is taken from the difference in the absolute energetic posi-

TABLE I. Material parameters used in the calculations. E_{gap} is the band gap (eV), C_{ij} are the compliances (10^{10} Pa), a, a_C, b, and d the deformation potentials (eV), and e_{14} the piezoelectric modul (C/m^2). Values are obtained from linear interpolation of values for the binaries. a and a_C are taken from Ref. 26, other values from Ref. 25. b, d, and e_{14} for $Al_{1-x}Ga_xAs$ have been taken as GaAs values.

Material	E_{gap}	C_{11}	C_{12}	C_{44}	a	a_C	b	d	e_{14}
$In_{0.2}Ga_{0.8}As$	1.222	11.4	5.3	5.6	−7.9	−6.8	−1.8	−4.0	0.137
$Al_{0.2}Ga_{0.8}As$	1.774	12.2	5.5	5.9	−8.3	−6.9	−1.9	−4.2	0.16

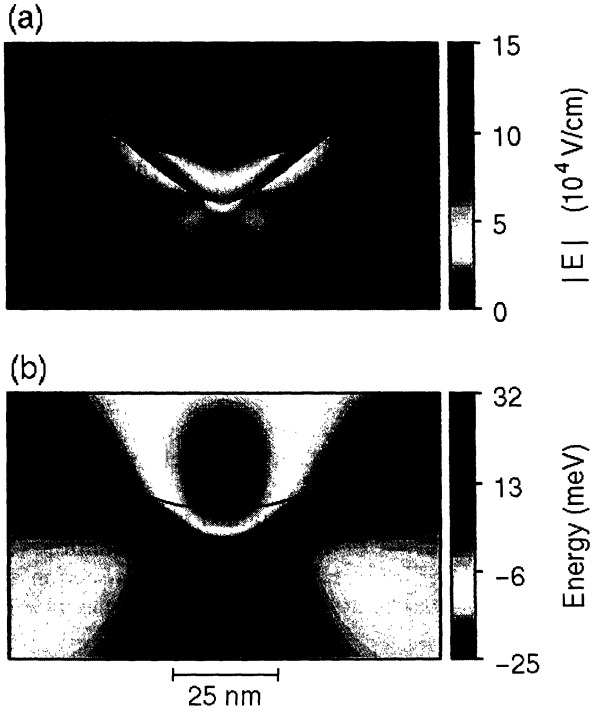

FIG. 4. Piezoelectric field amplitude (a) and piezoelectric potential for electrons (b) for an $In_{0.2}Ga_{0.8}As/Al_{0.2}Ga_{0.8}As$ quantum wire.

tion of the average valence band[26] and amounts to $Q_0=70\%$ for $In_{0.2}Ga_{0.80}As/Al_{0.2}Ga_{0.8}As$, taking into account the different spin-orbit splittings and alloy terms.[27] The hydrostatic shift E_0 is split between conduction and valence bands with a ratio $Q_\varepsilon=a_C/a$, a_C being the hydrostatic deformation potential for the conduction band obtained from model-solid theory.[26] In summary we obtain

$$\Delta E_e=Q_0\Delta E_{\text{gap}}+Q_\varepsilon E_0-eV_P\ , \tag{4}$$

$$\Delta E_h=(1-Q_0)\Delta E_{\text{gap}}+(1-Q_\varepsilon)E_0\pm\tfrac{1}{2}E_1+eV_P\ . \tag{5}$$

The piezoelectric potential V_P for the electrons is shown in Fig. 4 together with the magnitude of the piezoelectric field $|\mathbf{E}_P|$, $\mathbf{E}_P=-\text{grad}V_P$. The piezoelectric field depends on the wire shape but not on its particular size. In contrast, the piezoelectric potential depends linearly on the length scale and thus becomes increasingly stronger and more important for larger wires.

The resulting confinement potentials are depicted in Fig. 5. In the case of compressive strain as here, the upper-hole band has heavy-hole character, while the light hole is largely shifted away from the band edge. We will refer to the hole as heavy hole (hh) in the following. Contrary to the case of a quantum well, the barrier also becomes strained in the vicinity of the QWR, and the strain-induced potentials in the barriers are included into the band structure as well.

The important feature of the hole confinement potential is that its minimum is not located in the center of the V groove. Two equivalent minima exist in the left and right half of the QWR *(symmetry breaking)* for the holes. The minima are at lateral positions where the QWR thickness is tapered. It will therefore depend on the magnitude of the size quantization (which is a function of the wire size and the particle mass), how much the strain-induced potential influences the spectrum, the wave functions, and subsequently the recombination properties in

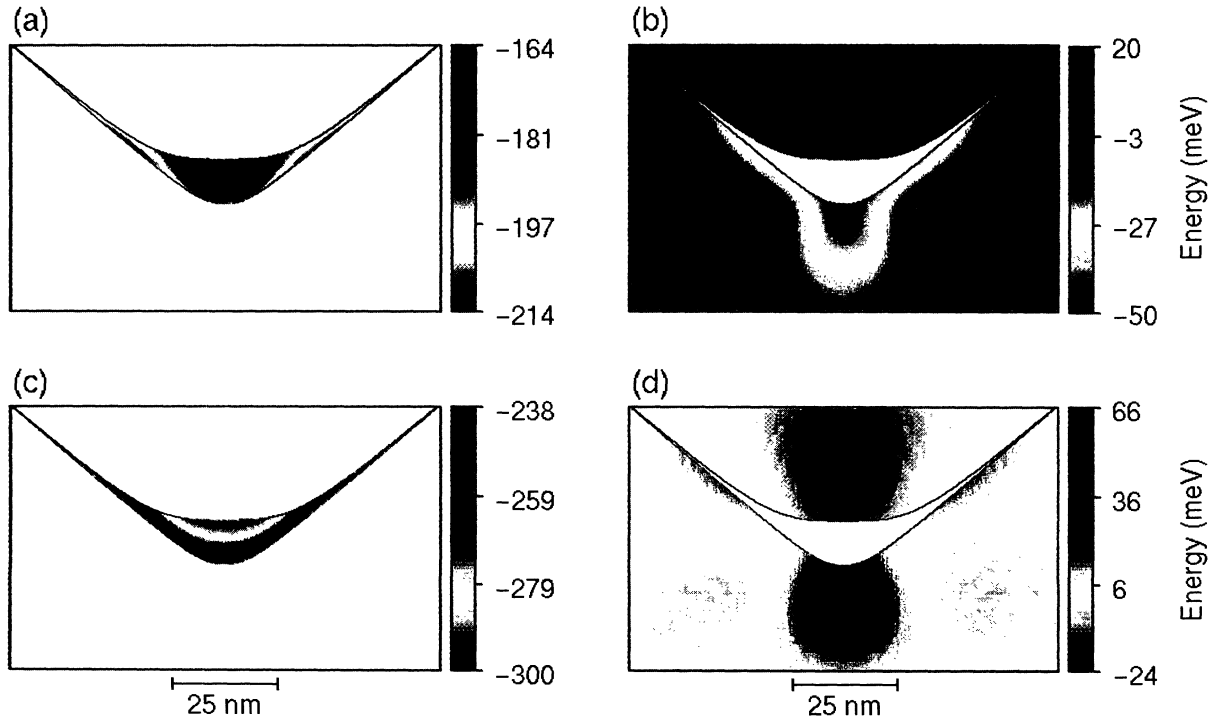

FIG. 5. Confinement potential for holes in the wire (a), and in the barrier (b) and electrons in the wire (c), and in the barrier (d) for an $In_{0.2}Ga_{0.8}As/Al_{0.2}Ga_{0.8}As$ quantum wire.

the QWR. For very small wires the strain will be a perturbation, while for large wires the spectrum will be dominated by the influence of the strain-induced potential. With larger lattice mismatch the influence of the symmetry-breaking potential will increase and also impact smaller wires.

For tensile material combinations, e.g., $In_xGa_{1-x}As/InP$, $x<0.53$, the fundamental band edge has light-hole character and the sign of E_0 changes. Thus the strain-induced potential for electrons has its position in the center of the groove, and the (light)-hole tensile strain-induced potential exhibits a similar symmetry breaking as that of (heavy) holes in the case of compressive strain.

To access the quantum-mechanical consequences of the strain-induced potentials we solve the Schrödinger equation for electrons and holes. We use a true two-dimensional, nonseparable ansatz with a linear combination of orthonormal functions,

$$\Phi_{ij}(x,z)=\frac{e^{-(x^2+z^2)/2}}{(\sqrt{\pi}i!j!2^{i+j})^{1/2}}H_i(x)H_j(z)\ , \tag{6}$$

where H_k is the kth Hermitian polynomial. The size of the basis is chosen to $i+j\le k$, $k=30$, giving the first six levels with sufficient accuracy. The barrier and well masses are taken identical and isotropic. We use $m_e=0.06$ and $m_{hh}=0.5$. We note that due to the mirror symmetry of the QWR potential the wave functions have well-defined parity. Due to the larger mass of the heavy hole, the strain-induced effects are more pronounced for the holes.

Before we present the results of the two-dimensional quantum-mechanical calculation we briefly like to treat the problem in the so-called adiabatic approximation,[4] In this scheme the lateral confinement energy $E_c(x)$ is calculated at each position by solving the Schrödinger equation in the z direction. This ansatz is a good approximation for laterally slowly varying potentials and is found to result in mainly a *shift* of eigenenergies, preserving the subband spacings for low-lying levels.[28] The lateral potentials for holes and electrons obtained from the adiabatic calculation for the confinement potentials of Fig. 5 is shown in Fig. 6. This reflects the two equivalent off-center minima for the holes.

The following results are obtained with the truly two-dimensional solution of the Schrödinger equation. For increasing QWR size (measured by the cross-section area at constant shape) the hole levels pairwise degenerate [see

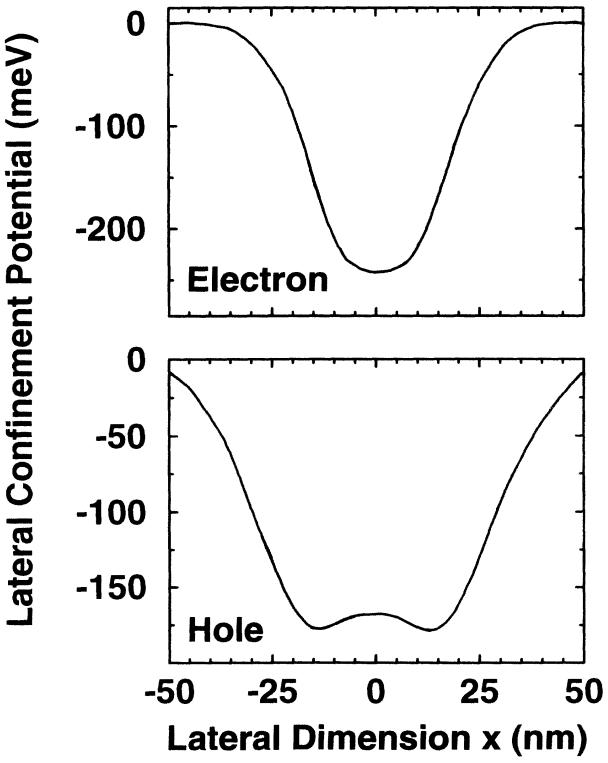

FIG. 6. Lateral confinement potentials for electrons and holes obtained from adiabatic approximation of the confinement potentials of Fig. 5.

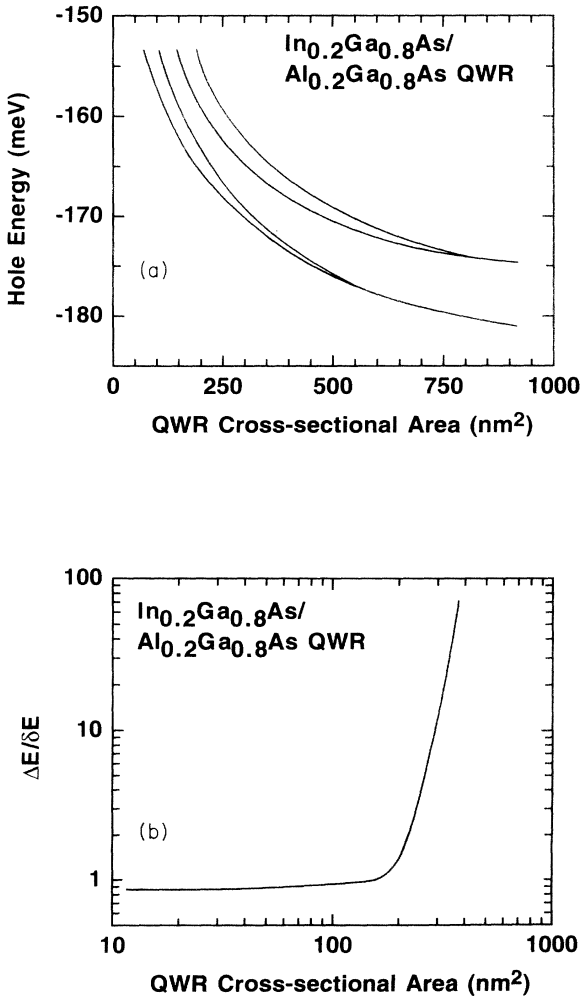

FIG. 7. First four hole energy levels (a) and their degeneracy (b) for an $In_{0.2}Ga_{0.8}As/As_{0.2}Ga_{0.8}As$ quantum wire.

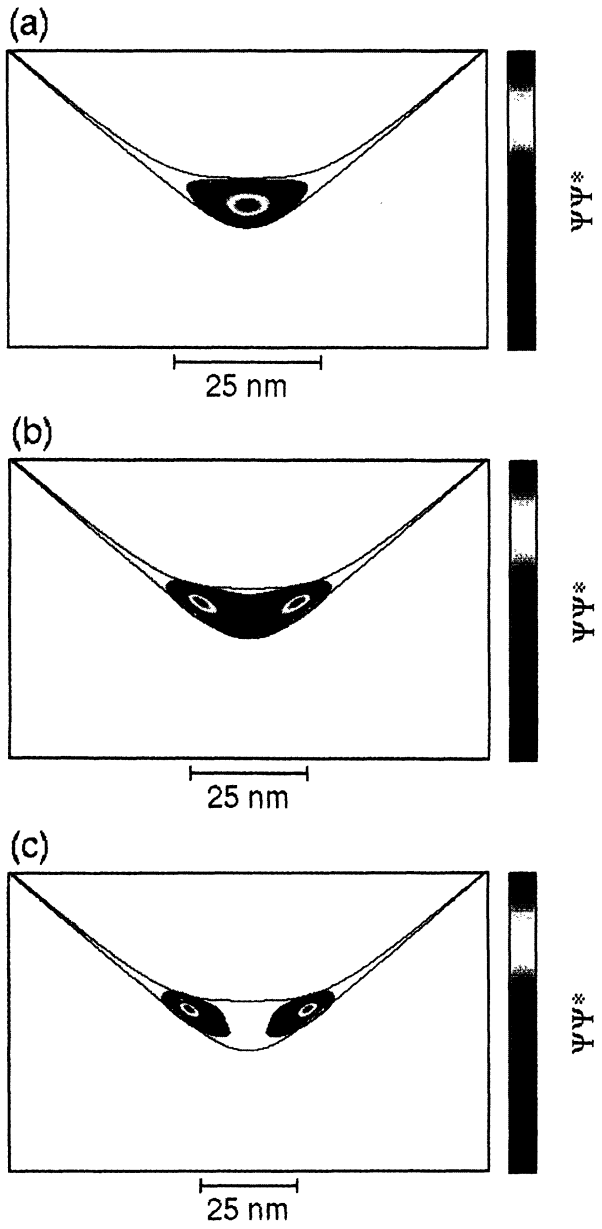

FIG. 8. Hole ground-state wave function for three different $In_{0.2}Ga_{0.8}As/Al_{0.2}Ga_{0.8}As$ wire sizes [cross-sectional area is 180 nm^2 (a), 290 nm^2 (b), and 400 nm^2 (c), respectively] showing the transition to symmetry breaking. Note different markers for each figure.

Fig. 7(a)]. The splitting δE between the $n=1$ and 2 levels becomes small compared to the energetic distance ΔE between the $n=2$ and the 3 level [see Fig. 7(b)]. Simultaneously the ground-state wave function of the holes becomes bimodal and shows a well-defined minimum in the center of the groove (see Fig. 8). In the regime of strong symmetry breaking the $n=1$ and 2 heavy hole wave functions are symmetric and antisymmetric states of two weakly coupled oscillators. Introducing a basis set of wave functions

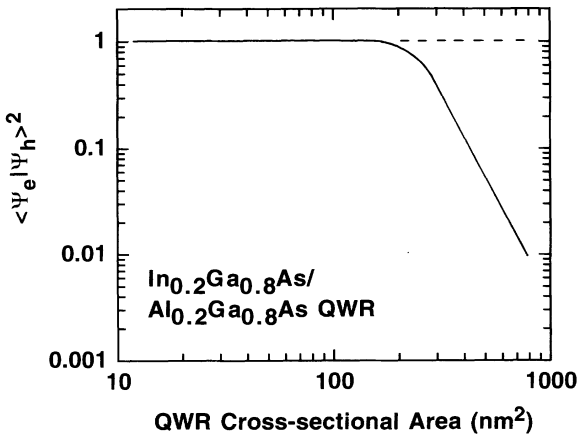

FIG. 9. Overlap integral between hole and electron ground-state wave function for an $In_{0.2}Ga_{0.8}As/Al_{0.2}Ga_{0.8}As$ quantum wire.

$$|l\rangle=\frac{1}{\sqrt{2}}(|1\rangle+|2\rangle) \text{ and } |r\rangle=\frac{1}{\sqrt{2}}(|1\rangle-|2\rangle),$$

the situation can be viewed as if the heavy hole is either in the left or the right half of QWR. It will oscillate with a tunneling time $\tau\approx h/(2\delta E)$, which is $\tau\approx 20$ ps for $\delta E=0.1$ meV. We expect a different type of quantum beat in this system. Due to the much smaller electron mass the electron levels are almost not impacted by the strain and the wave functions show no symmetry breaking.

Radiative transitions between electron and hole levels are allowed only between states of the same parity of the envelope functions. Due to the strain-induced symmetry breaking for the holes the wave-function overlap with the electrons is reduced, and thus the carrier lifetime will be increased by the strain effects. In Fig. 9 we show the QWR size dependence of the overlap of the envelope ground-state wave functions $\langle\Psi_e|\Psi_{hh}\rangle^2$ which is proportional to the recombination lifetime. It is obvious that the lifetime becomes substantially decreased for increasing wire size. Our treatment so far neglects excitonic effects which will be studied in subsequent work. The size dependence of the carrier lifetime is, however, found to be profoundly changed by the inclusion of strain effects.

In summary, we have shown that pseudomorphic nanostructures require a detailed analysis of their strain distribution and its consequences on the electronic properties. In particular, crescent-shaped quantum wires exhibit size-dependent symmetry breaking of the hole wave function manifesting itself in level degeneracies. The recombination properties are largely affected; we predict increased carrier lifetime and a different type of quantum beat.

We are indebted to V. Türck for valuable discussions and numerical assistance. Part of this work was funded by Deutsche Forschungsgemeinschaft in the framework of Sfb 296.

[1]G. C. Osbourne, Phys. Rev. B **27**, 5126 (1989).
[2]L. D. Nguyen, D. C. Radulescu, M. C. Foisy, P. J. Tasker, and L. F. Eastman, IEEE Trans. Electron. Devices **36**, 833 (1989).
[3]P. K. York, K. J. Beernink, G. E. Fernández, and J. J. Coleman, Appl. Phys. Lett. **54**, 499 (1989).
[4]E. Kapon, D. M. Hwang, and R. Bhat, Phys. Rev. Lett. **63**, 430 (1989).
[5]M. Kohl, D. Heitmann, P. Grambow, and K. Ploog, Phys. Rev. Lett. **63**, 2124 (1989).
[6]M. Walther, E. Kapon, C. Caneau, D. M. Hwang, and L. M. Schiavone, Appl. Phys. Lett. **62**, 2170 (1993).
[7]T. Arakawa, M. Nishioka, Y. Nagamune, and Y. Arakawa, Appl. Phys. Lett. **64**, 2200 (1994).
[8]J. M. Moison, F. Houzay, F. Barthe, L. Leprince, E. André, and O. Vatel, Appl. Phys. Lett. **64**, 196 (1994).
[9]D. Leonard, M. Krishnamurthy, C. M. Reaves, S. P. Denbaars, and P. M. Petroff, Appl. Phys. Lett. **63**, 3203 (1993).
[10]A. Yu. Egorov, A. E. Zhukov, P. S. Kop'ev, N. N. Ledentsov, M. V. Maksimov, and V. M. Ustinov, Fiz. Tekh. Poluprovodn. **28**, 604 (1994) [Semiconductors **28**, 363 (1994)].
[11]K. Kash, B. P. Van der Gaag, D. D. Mahoney, A. S. Gozdz, L. T. Florez, J. P. Harbison, and M. D. Sturge, Phys. Rev. Lett. **67**, 1326 (1991).
[12]D. Gershoni, J. S. Weiner, S. N. G. Chu, G. A. Baraff, J. M. Vandenberg, L. N. Pfeiffer, K. West, R. A. Logan, and T. Tanbun-Ek, Phys. Rev. Lett. **65**, 1631 (1990).
[13]J. Christen, M. Grundmann, E. Kapon, E. Colas, D. M. Hwang, and D. Bimberg, Appl. Phys. Lett. **61**, 67 (1992).
[14]M. Grundmann, J. Christen, M. Joschko, O. Stier, D. Bimberg, and E. Kapon, Semicond. Sci. Technol. **9**, 1939 (1994).
[15]This is true for infinitely thick substrates; otherwise substrate bending occurs whose influence can be completely neglected in this work.
[16]G. L. Bir and G. E. Pikus, *Symmetry and Strain-Induced Effects in Semiconductors* (Wiley, New York, 1974).
[17]F. H. Pollak, Semicond. Semimet. **32**, 17 (1990).
[18]F. H. Pollak and M. Cardona, Phys. Rev. **172**, 172 (1968).
[19]W. F. Cady, *Piezoelectricity* (McGraw-Hill, New York, 1946).
[20]D. L. Smith and C. Mailhiot, J. Appl. Phys. **63**, 2717 (1988).
[21]E. A. Caridi, T. Y. Chang, K. W. Goossen, and L. F. Eastman, Appl. Phys. Lett. **56**, 659 (1990).
[22]R. P. Mirin, I-H. Tan, H. Weman, M. Leonard, T. Yasuda, J. E. Bowers, and E. L. Hu, J. Vac. Sci. Technol. A **10**, 697 (1992).
[23]T. Arakawa, S. Tsukamoto, Y. Nagamune, M. Nishioka, J.-H. Lee, and Y. Arakawa, Jpn. J. Appl. Phys. **32**, L1377 (1993); T. Arakawa, M. Nishioka, Y. Nagamune, and Y. Arakawa, Appl. Phys. Lett. **64**, 2200 (1994).
[24]M. Grundmann, V. Türck, J. Christen, E. Kapon, C. Caneau, R. Bhat, and D. Bimberg, Solid State Electron. **37**, 1097 (1994).
[25]*Physics of Group IV Elements and III-IV Compounds,* edited by O. Madelung, Landolt-Börnstein, New Series, Group III, Vol. 17, Pt. a (Springer-Verlag, Berlin, 1982).
[26]Ch. G. Van der Walle, Phys. Rev. B **39**, 1871 (1989).
[27]M. Cardona and N. E. Christensen, Phys. Rev. B **37**, 1011 (1988).
[28]O. Stier, M. Grundmann, and D. Bimberg (unpublished).

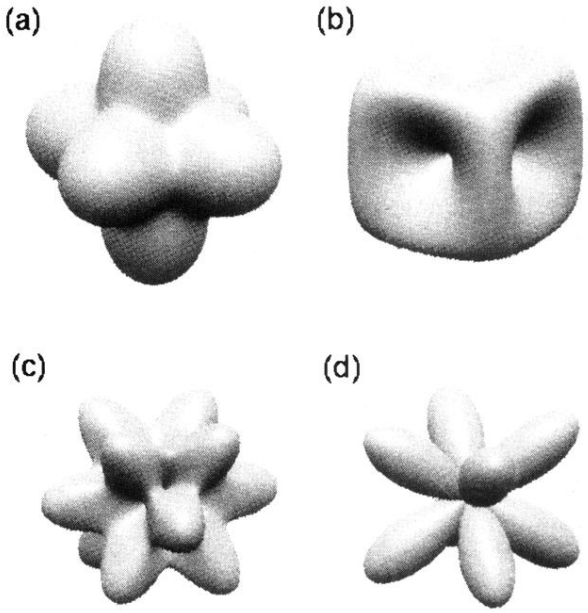

FIG. 2. Three-dimensional visualization of c_p (a), P_0 (b), $P_0^{\parallel}$ (c), and $P_0^{\perp}$ (d). For a description of symbols see caption of Fig. 1 and text. $\langle 100 \rangle$ directions are along maxima in (a), $\langle 111 \rangle$ directions are along maxima in (d).

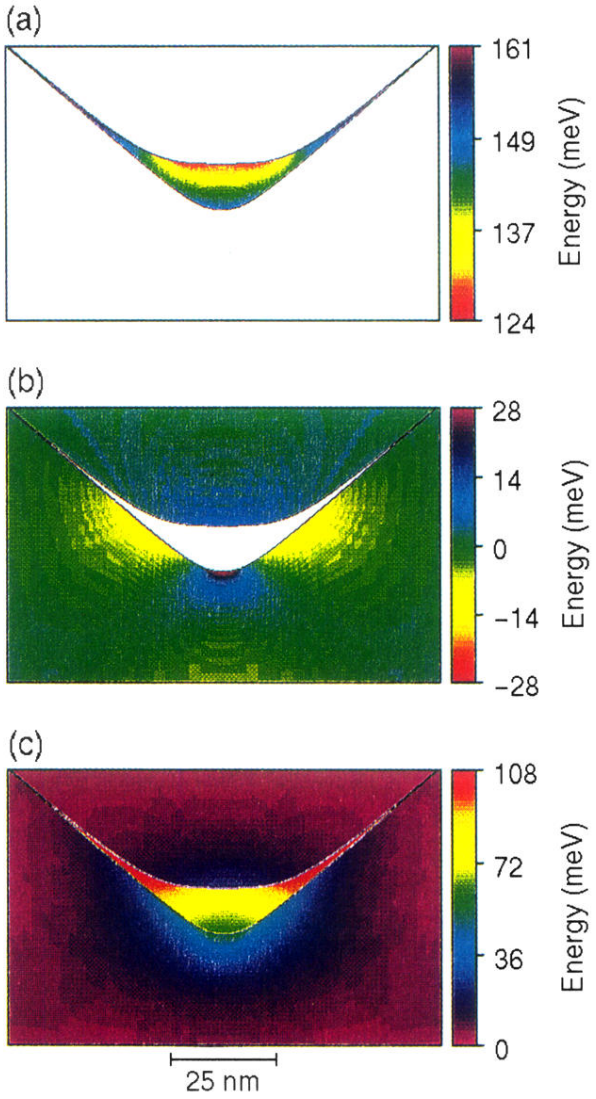

FIG. 3. Hydrostatic band shift in the wire (a), and in the barrier (b), and valence-band splitting (c) for an $In_{0.2}Ga_{0.8}As/Al_{0.2}Ga_{0.8}As$ quantum wire. Color scale for (c) is reversed because larger valence-band splitting means lower hole ground-state energy.

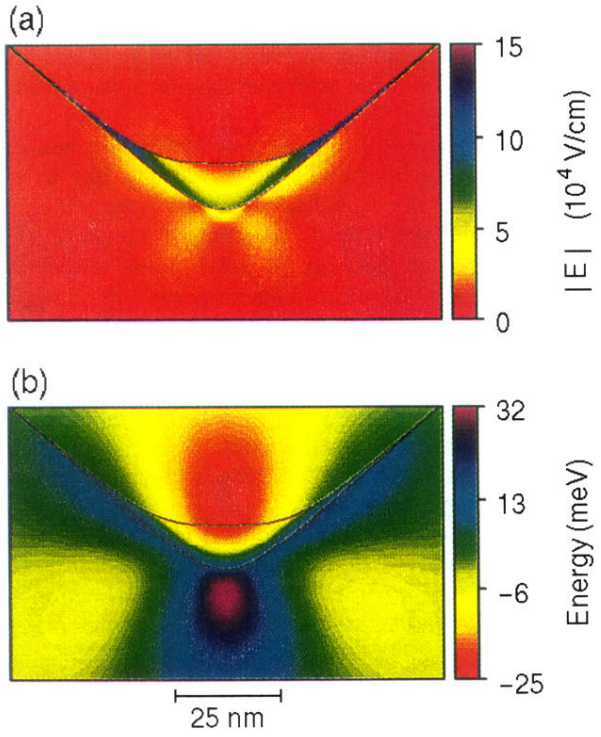

FIG. 4. Piezoelectric field amplitude (a) and piezoelectric potential for electrons (b) for an $In_{0.2}Ga_{0.8}As/Al_{0.2}Ga_{0.8}As$ quantum wire.

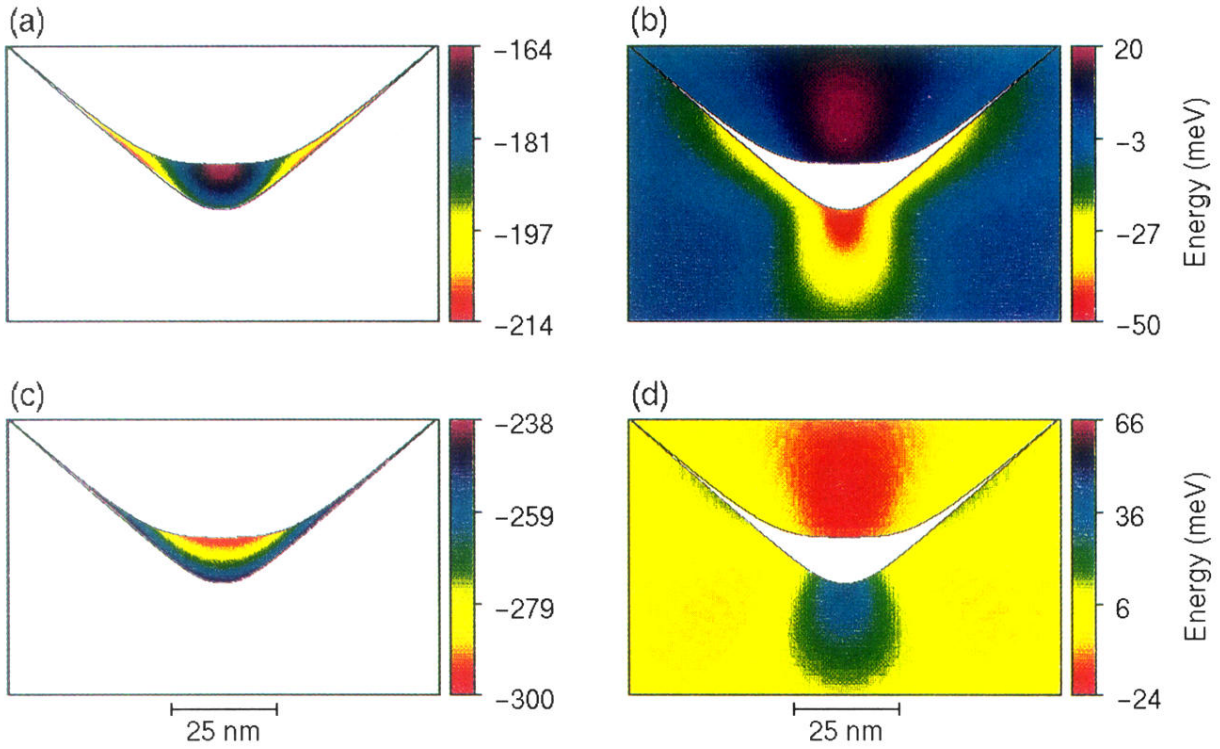

FIG. 5. Confinement potential for holes in the wire (a), and in the barrier (b) and electrons in the wire (c), and in the barrier (d) for an $In_{0.2}Ga_{0.8}As/Al_{0.2}Ga_{0.8}As$ quantum wire.

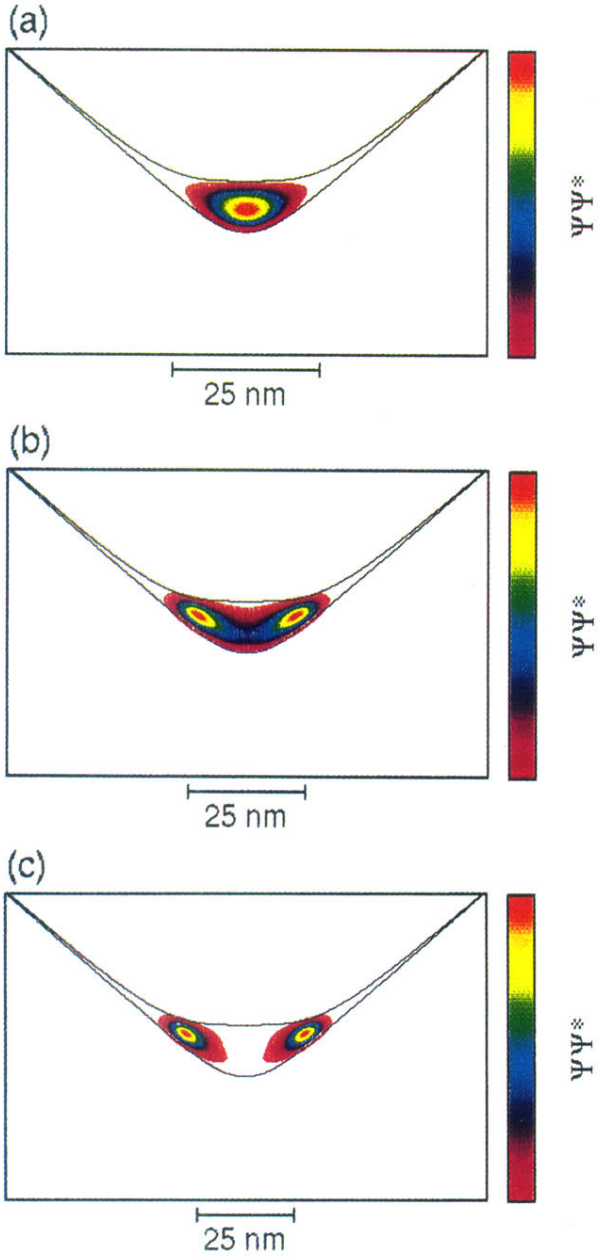

FIG. 8. Hole ground-state wave function for three different $In_{0.2}Ga_{0.8}As/Al_{0.2}Ga_{0.8}As$ wire sizes [cross-sectional area is 180 nm^2 (a), 290 nm^2 (b), and 400 nm^2 (c), respectively] showing the transition to symmetry breaking. Note different markers for each figure.